Journal of Power Sources 244 (2013) 177–182

Contents lists available at SciVerse ScienceDirect

Journal of Power Sources

journal homepage: www.elsevier.com/locate/jpowsour

Synthesis of Fe_3O_4/C composite microspheres for a high performance lithium-ion battery anode

Byung-Young Jung [a], Hyung-Seok Lim [a], Yang-Kook Sun [b,**], Kyung-Do Suh [a,*]

[a] Department of Chemical Engineering, College of Engineering, Hanyang University, Seoul 133-791, Republic of Korea
[b] Department of WCU Energy Engineering, College of Engineering, Hanyang University, Seoul 133-791, Republic of Korea

HIGHLIGHTS

- We prepare Fe_3O_4/C composite microspheres containing high content of Fe_3O_4.
- We examine the electrochemical performances depending on the particle morphologies.
- Our particle structure effectively suppresses the aggregation of Fe_3O_4 nanoparticles.
- Surface modified-Fe_3O_4 nanoparticles can be uniformly embedded in carbon matrix.

ARTICLE INFO

Article history:
Received 8 November 2012
Received in revised form
27 January 2013
Accepted 13 February 2013
Available online 27 February 2013

Keywords:
Iron oxide/carbon composite
Alternative anode materials
High content of magnetite
Particle morphology
Lithium-ion batteries

ABSTRACT

Fe_3O_4/carbon (Fe_3O_4/C) composite microspheres with a high content of Fe_3O_4 nanoparticles as an active material are prepared by suspension polymerization and heat treatment. A significant difference is observed in the morphology of the Fe_3O_4/C composite microspheres with the introduction of different amounts of Fe_3O_4 nanoparticles. The morphological and structural differences of the Fe_3O_4/C composite microspheres are characterized by focused ion beam cross-section, scanning electron microscopy, transmission electron microscopy, and X-ray diffraction analysis. Thermogravimetric analysis is conducted to measure the amount of Fe_3O_4 nanoparticles introduced into a carbon matrix. We fix two samples with Fe_3O_4 contents of 72 wt.% and 98 wt.%, respectively. Fe_3O_4/C composite microspheres containing 72 wt.% Fe_3O_4 nanoparticles show much higher capacity retention with an excellent columbic efficiency of 99% at every cycle in comparison with that of the Fe_3O_4/C composite microspheres containing 98 wt.% Fe_3O_4 nanoparticles when used as anodes for LIBs. These results indicate that the particle morphology and weight ratio of incorporated Fe_3O_4 to carbon matrix affects the electrochemical performance of Li-ion cells.

1. Introduction

Graphite is currently used commercially as the anode active material for lithium-ion batteries (LIBs) because of its good cycling stability and high columbic efficiency. However, the low intrinsic specific capacity and low energy density of LIBs cannot satisfy the needs of future applications such as electric devices and vehicles with high power requirements [1]. In the past few years, various materials have been studied as potential anode alternatives for LIBs [2–6]. Among these alternatives, transition metal oxides (MO) have been developed for use in novel anodes because they have a high specific capacity from the conversion mechanism without an intercalation reaction. Magnetite (Fe_3O_4) anodes have attracted great attention for next-generation LIBs because of their much higher theoretical capacity (927 mAh g^{-1}) than that of conventional graphite anodes (372 mAh g^{-1}), low cost, increased safety, and environmental benignity [7,8]. Unfortunately, Fe_3O_4 anodes also display poor cycling performance, especially at high rates, because the repeated volume change of Fe_3O_4 anodes during lithiation/delithiation breaks down the electrical conduction of electrodes [7,9]. Nano-sized Fe_3O_4 powder has recently been employed in anodes to accommodate volume variation and improve rate capability by increasing active reaction sites [8,10–14]. However, they show large irreversible capacity at the first cycle and gradual capacity fading during continuous cycling due to electrolyte decomposition and nanoparticle aggregation during the Li-ion reaction.

* Corresponding author. Tel.: +82 2 2220 0526; fax: +82 2 2220 4680.
** Corresponding author. Tel.: +82 2 2220 1749; fax: +82 2 2298 5416.
E-mail addresses: yksun@hanyang.ac.kr (Y.-K. Sun), kdsuh@hanyang.ac.kr (K.-D. Suh).

0378-7753/$ – see front matter © 2013 Elsevier B.V. All rights reserved.
http://dx.doi.org/10.1016/j.jpowsour.2013.02.035

Many research groups have prepared Fe_3O_4/amorphous carbon composite materials that have shown improved electrochemical performance [7–9,15–17].

We prepared Fe_3O_4/C composite microspheres with a high Fe_3O_4 nanoparticle content as an active material and evaluated them as anode material for high performance LIBs. The Fe_3O_4 nanoparticles were synthesized by a co-precipitation method, and a large amount of Fe_3O_4 nanoparticles could be introduced into the poly(acrylonitrile-co-3-(trimethoxysilyl)propyl methacrylate) (poly(AN-co-TMSPM)) matrix by suspension polymerization, which had different morphologies depending on the weight ratio of Fe_3O_4 nanoparticles to polymer matrix. After heat treatment, a black powder was obtained which was used as the anode electrode in coin-type cells. The electrochemical performance of the Fe_3O_4/C composite microspheres was evaluated, and the Fe_3O_4/C composite microspheres containing 72 wt.% Fe_3O_4 nanoparticles showed a high reversible capacity of 500 mAh g^{-1} at 1 C with an excellent columbic efficiency of 99% even after 300 cycles.

2. Experimental

2.1. Materials

Acrylonitrile (AN, JUNSEI, Chuo-ku, Tokyo, Japan), 2,2′-azobis-(2,4-dimethylvaleronitrile) (ADVN, Waco Chemical Co., Dalton, GA, United States), 3-(trimethoxysilyl)propyl methacrylate (TMSPM, 98%, ALDRICH Chemical Co., Milwaukee, WI, United States), Methylene Chloride (MC, DAEJUNG Chemicals & Metals Co., Siheung Si, Gyeonggi-do, Korea), Poly(vinyl alcohol) (PVA, avg. Mw. 85,000–124,000, 87–89% hydrolyzed, Sigma ALDRICH Chemical Co., Milwaukee, WI, United States), Di-2-ethylhexyl sodium sulfosuccinate (Aerosol® OT, Wako Chemical, Dalton, GA, United States), Iron (III) Chloride, Anhydrous ($FeCl_3$, Showa), Iron (II) Chloride Tetrahydrate ($FeCl_2 \cdot 4H_2O$, Wako), and Citric Acid (CA, S.P.C GR Reagent, SAMCHUN PURE CHEMICAL INDUSTRIES LTD) were used as received.

2.2. Preparation of Fe_3O_4 nanoparticles

Fe_3O_4 nanoparticles were prepared with citric acid by co-precipitation of a $FeCl_2$ and $FeCl_3$ (1:2 M ratio) salt solution by the addition of NH_4OH [18]. In a typical synthesis, 0.86 g of $FeCl_2$ and 2.35 g of $FeCl_3$ were dissolved in 40 mL of DI water in a four-neck flask equipped with a condenser and nitrogen inlet system with constant mechanical stirring at 400 rpm at 80 °C. 10 mL of NH_4OH was then slowly added to the salt solution and heated for 30 min. Afterward, 2 mL of water containing 1 g of citric acid was added into the reactor and heated to 95 °C with additional stirring for 90 min. When the above procedure was finished, the reaction mixture was cooled to room temperature under nitrogen injection. The black precipitates were separated and rinsed magnetically about three times with DI water, and dialysis was conducted over approximately 72 h by the periodic exchange of DI water. Very fine Fe_3O_4 nanoparticles were obtained after freeze-drying.

2.3. Preparation of Fe_3O_4/C composite microsphere

First, 2 g of TMSPM and 0.5 g or 1.0 g Fe_3O_4 nanoparticles were put into a 250 mL four-neck glass reactor containing 30 g of methylene chloride (MC). To disperse the aggregated nanoparticles in the mixture, the reactor was sonicated on ice for 1 h. 10 g of acrylonitrile (AN) containing 0.1 g of ADVN was then added into the reactor, and immersed in a 55 °C pre-heated oil bath equipped with a nitrogen inlet system and condenser. After constant stirring at 300 rpm for 2 h, the polymerized mixture was dripped slowly into the polymeric solution, which contained 500 mL of PVA 2 wt.% and Aerosol OT 1 wt.%, and stirred vigorously at ambient temperature for 12 h. The resultant precipitates were washed with DI water and freeze-dried. Dried particles were heated to 670 °C at 5 °C min^{-1} and maintained for 3 h at 670 °C under nitrogen atmosphere.

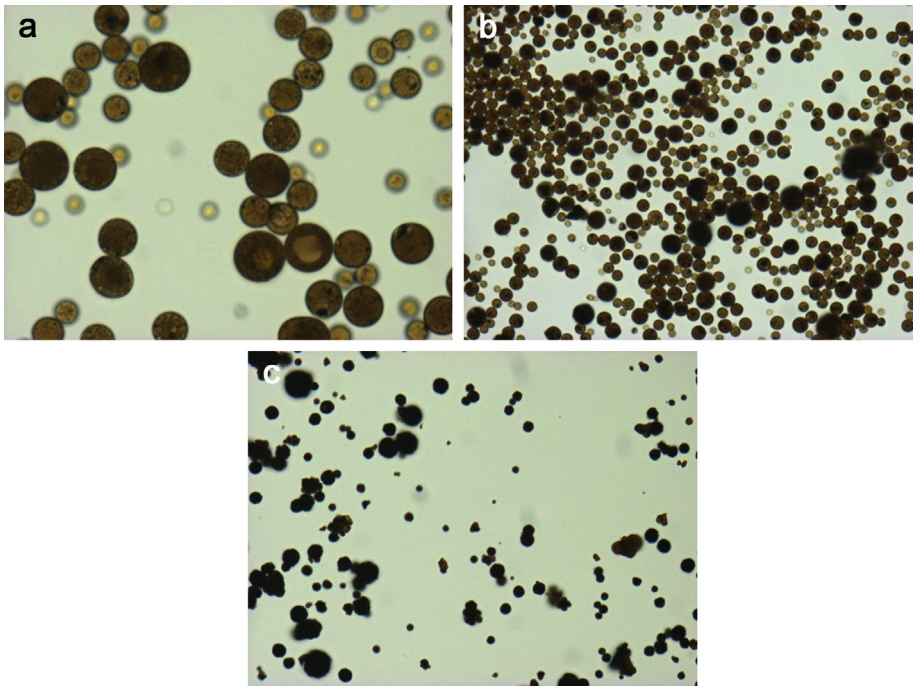

Fig. 1. OM images of (a) S1001, (b) S1005 and (c) S1010 stabilized in water containing PVA and Aerosol OT.

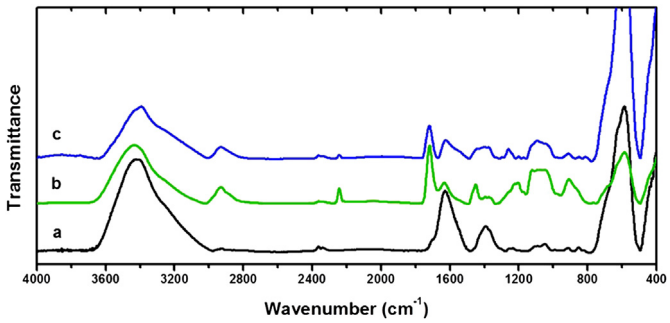

Fig. 2. FT-IR spectra of (a) Fe_3O_4 nanoparticles, (b) S1005, and (c) S1010.

2.4. Characterization of materials

The average size of as-prepared Fe_3O_4 nanoparticles in the mixture was measured by a Zetasizer (Nano ZS, Malvern). Fourier transform infrared spectroscopy (FT-IR, Nicolet, Mahgna IR-550) analysis was conducted to verify the chemical bonding components. Morphologies and structures of the composite microspheres were observed by optical microscopy (OM, OlympusBH-2), scanning electron microscopy (SEM, JSM-6300, JEOL), and transmission electron microscopy (TEM, TEM 2100F, JEOL). A TEM sample was prepared by dispersion in methanol and deposition onto a 50 mesh Cu grid, and energy-dispersive X-ray spectroscopy (EDX) mapping. Thermo-gravimetric analysis (TGA, TG209F3, NETZSCH) was used to identify the compositions of magnetite and carbon in the composite microspheres. In order to estimate the ratio of Fe_3O_4 to amorphous carbon, TGA measurement was conducted under air atmosphere. TGA curves of S1005 and S1010 indicated that S1005 and S1010 have different Fe_3O_4 nanoparticle contents. At the end of measurement, the residual Fe_3O_4 contents of S1005 and S1010 were 72 wt. % and 98 wt. %, respectively. In the case of S1010, since Fe_3O_4 nanoparticles were partially exposed from their carbon matrix, and a slight mass increase was observed in the range of 200 °C–300 °C by the transformation of the crystallinity of Fe_3O_4 nanoparticles.

The crystalline phases of the microsphere were confirmed by X-ray powder diffraction (XRD, Bruker) using Cu Kα radiation ($\lambda = 1.542$ Å) in the 2θ range.

2.5. Electrochemical performance test

The electrochemical performance of as-prepared Fe_3O_4/C composite microsphere was evaluated by fabricating a 2032 coin-type cell. The working electrodes were prepared by mixing active materials (60 wt.%, Fe_3O_4/C composite microspheres) and Super-P (20 wt.% as the conductive additive) with PVDF (20 wt.%). The slurry was then cast onto pure Cu foil and dried in an oven at 110 °C for 20 min. The electrodes were pressed by a roll pressing machine and dried in a vacuum oven at 80 °C for 3 h. Coin-type cells (2032) were assembled in an argon-filled glove box. We used pure Li metal as the counter electrode, Celgard 2400 polyethylene as a separator, and ethylene carbonate and diethylene carbonate (EC:DEC, 1:1 by volume, provided by Techno Semichem Co. Ltd., Korea) containing 1 M $LiPF_6$. Cyclic voltammograms (CV) were carried out over a 0.01–3.5 V voltage window and with a scan rate of 0.5 mV s^{-1} (CH Instrument, WonATech). In order to measure the cycleability of the cell, the cycling test was performed over a voltage range of 0.02–3.0 V (vs Li/Li^+) at current rates of 0.2 C and 1 C by the Basytest battery test program (BaSyTec), and rate capability was measured at a high-speed charge/discharge rate of 0.2 C–10 C.

3. Results & discussion

3.1. Characterization of prepared microspheres

We summarized sample names as the weight of Fe_3O_4 nanoparticles and their characteristics, as shown in Table 1. As-

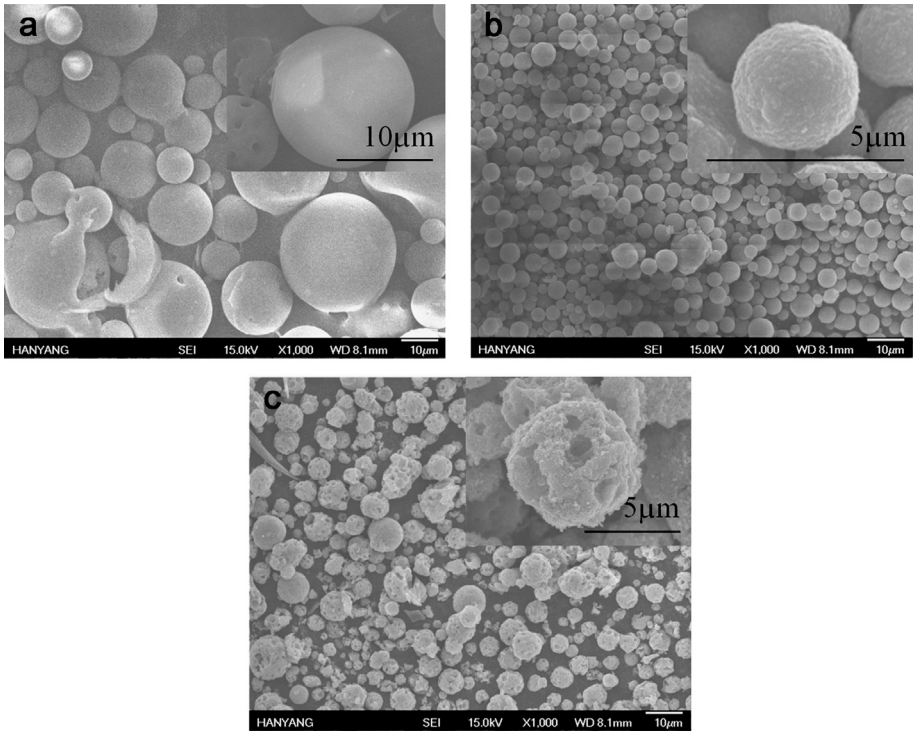

Fig. 3. SEM images of (a) S1001, (b) S1005 and (c) S1010 after heat treatment at low and (insets) high magnification.

Table 1
Characteristics of the final microspheres prepared with the different content of Fe_3O_4 nanoparticles.

Sample	Fe_3O_4 nanoparticles (Weight/g)	Acrylonitrile (Weight/g)	TMSPM (Weight/g)	Average diameter (μm)
S1001	0.1	10	2	23.82
S1005	0.5	10	2	5.64
S1010	1	10	2	6.31

synthesized Fe_3O_4 nanoparticles were characterized by SEM, TEM, and XRD, as shown in Fig. S1. The SEM and TEM (inset) images show clusters composed of Fe_3O_4 nanoparticles ranging in size from 30 nm to 50 nm, as shown in Fig. S1a. The XRD pattern of Fe_3O_4 nanoparticles demonstrates that the synthesized Fe_3O_4 nanoparticles have typical magnetite crystallinity, as shown in Fig. S1b.

Fig. 1 shows OM images of Fe_3O_4/poly(AN-co-TMSPM) composite microspheres with different amounts of incorporated Fe_3O_4 nanoparticles at the end of the stabilization period in PVA and Aerosol OT solution. S1010 (c) exhibits a darker color than S1001 (a) and S1005 (b), revealing that S1010 contains more Fe_3O_4 nanoparticles in the polymer matrix due to the fact that a large amount of Fe_3O_4 nanoparticles was combined with the polymer chains during the polymerization stage. S1010 and S1005 display a spherical shape and have similar size distributions while S1001 has much larger size and broad size distribution.

Fig. 2 shows FT-IR spectra of as-synthesized Fe_3O_4, S1005, and S1010. As shown in Fig. 2a, the 1715 cm^{-1} and 1369 cm^{-1} peaks corresponding to C=O vibration of the COOH group of CA were shifted to 1629 cm^{-1} and 1450 cm^{-1}, respectively, due to the combination of CA to the surface of the Fe_3O_4 nanoparticles. The peak of 588 cm^{-1} means well-synthesis of Fe_3O_4 as the Fe–O bond [18,19]. The FT-IR spectra of S1005 and S1010 shows several peaks which are associated with C–H, C=O, Si–C, and C–O–C corresponding to TMSPM at 2932 cm^{-1}, 1720 cm^{-1}, 1203 cm^{-1}, and 904 cm^{-1}, respectively, as shown in Fig. 2b and c. An absorption band of 1650 cm^{-1}, which would correspond to TMSPM C=C, was not observed, implying that TMSPM reacted completely with AN [20]. A peak was observed in both samples at around 2242 cm^{-1}, which is related to the presence of nitrile groups in the poly(AN-co-TMSPM) chain.

Fig. 3 shows SEM images of carbonized S100, S1005 and S1010. The S1001 has larger average diameter than those of S1005 and 1010 due to the small amount of CA-Fe_3O_4 nanoparticles. Fig. 3b and c shows that S1005 and S1010 have different surface morphologies, with S1010 having many potholes, while S1005 has a relatively smooth surface under high magnification (inset). In addition, the samples both have very different internal structures. Figure S3a and b shows that S1005 is filled with carbon and well-defined Fe_3O_4 nanoparticles, while S1010 has a sponge-like structure with macropores. The macroporous structure of S1010 might be caused by evaporation of MC and formation of a relatively small amount of poly(AN-co-TMSPM) during polymerization. Carbonized S1005 and S1010 showed the typical XRD patterns of magnetite, indicating the crystallinity of Fe_3O_4 nanoparticles in the carbon matrix was unchanged even after heat treatment under nitrogen atmosphere, as shown in Fig. S2.

Fig. 4 shows HR-TEM images of carbonized S1005 and S1010 at high magnification. As shown in Fig. 4a, Fe_3O_4 nanoparticle is surrounded by amorphous carbon layer that has the thickness of about 10 nm. On the other hand, S1010 showed Fe_3O_4 nanoparticles surrounded with very thin carbon layer of 0.51 nm, as shown in Fig. 4b. S1005 and S1010 show lattice fringe with *d*-spacing of 0.25 nm and 0.14 nm corresponding to the (311) and (511) planes of face-centered Fe_3O_4, respectively. The crystalline phases of all samples were unchanged after carbonization, as mentioned above and shown in Fig S2.

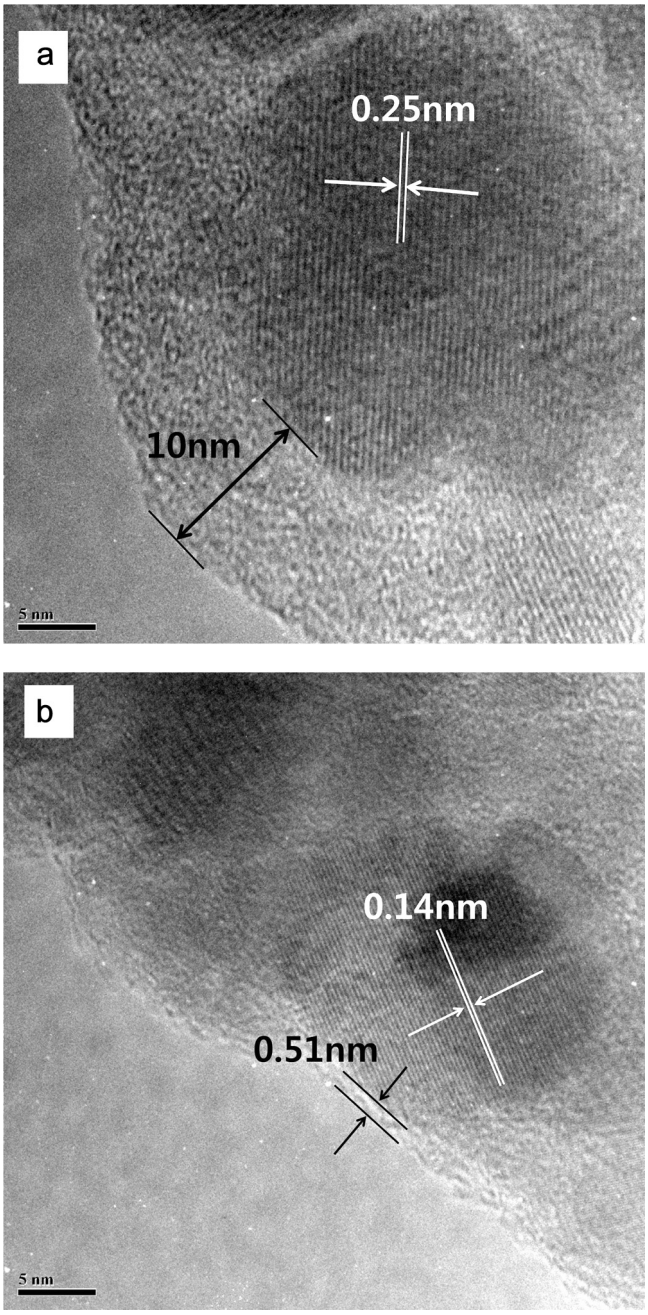

Fig. 4. TEM images of the heat-treated (a) S1005 and (c) S1010 at high magnification.

3.2. Electrochemical performance

The electrochemical properties of Fe_3O_4/C composite microspheres were investigated by cyclic voltammetry (CV) and a galvanostatic cycling test. Fig. 5 shows the cyclic voltammetry (CV) profiles of S1005 (a) and S1010 (b) for the initial 4 cycles in the voltage range between 3.5 V and 0.01 V at a scan rate 0.5 mV s^{-1}. Obvious peaks appeared at 0.55 V in the first cathodic process for S1005 and S1010. The broad peaks were located at 1.7–1.86 V in the first anodic process for both samples. In the second cycle, the cathodic peaks for both electrode materials shifted slightly due to polarization, and the decreased intensity of the cathodic peak for S1010 was much higher than that of S1005. This significantly larger irreversible capacity may be attributed to the higher specific surface area of S1010 having porous structure

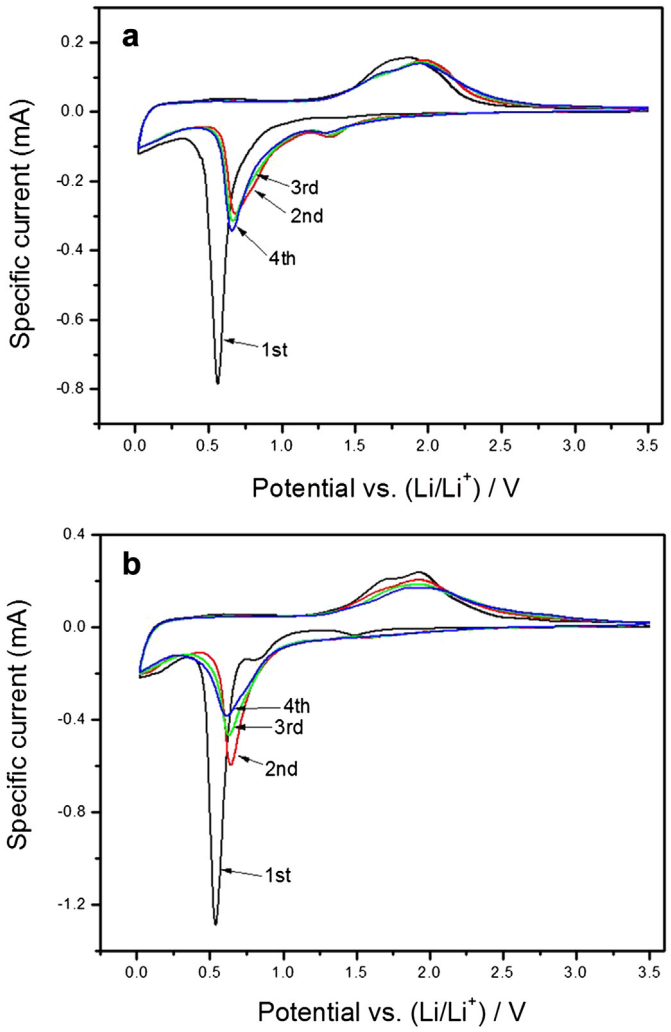

Fig. 5. Cyclic voltammograms of (a) S1005 and (b) S1010 with a scan rate of 0.5 mV s^{-1}. The cyclic numbers are indicated in the graph.

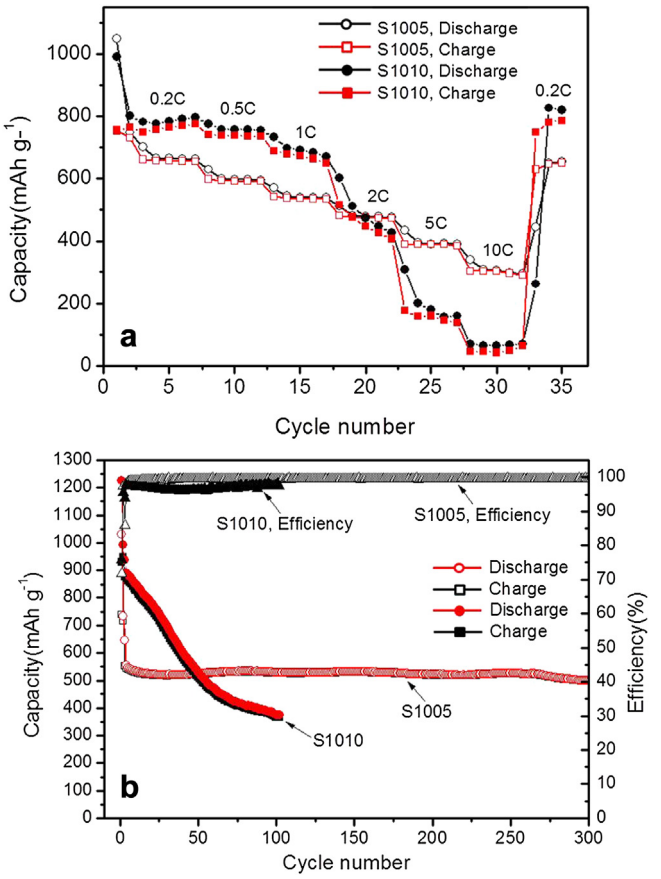

Fig. 6. Electrochemical performance of Fe_3O_4/C cells: (a) the specific capacity of S1005 (empty circles and squares) and S1010 (filled circles and squares) electrodes as a function of the cycling rate (0.2–10 C), and (b) cycling performance of S1005 (empty circles and squares) and S1010 (filled circles and squares) electrodes in the 0.02–3 V voltage window at 1 C.

than that of S1005. This irreversible capacity loss may be attributed to the formation of solid electrolyte interface (SEI) film during the first cycle, which is common for most anode materials.

The rate capability of the Fe_3O_4/C composite microspheres was evaluated at various currents up to 10 C to a cut-off voltage between 0.02 V and 3.5 V, as shown in Fig. 6a. Both S1005 and S1010 electrodes show good rate capability at low rates (0.2 C and 0.5 C). However, at high currents (from 1 C to 10 C), S1005 showed extremely stable cycling performance (even at 10 C), while S1010 showed poor cyclability, as mentioned in above Experimental section. These results are assumed to be due to the very small amount of carbon surrounding Fe_3O_4 nanoparticles and its low electrical conductivity. The cycling performances of S1005 and S1010 were evaluated at 1 C up to 300 and 100 cycles, respectively. The S1010 showed a higher discharge capacity of 1225 mAh g^{-1} at the first cycle due to its higher Fe_3O_4 nanoparticle content. However, the reversible specific capacities faded rapidly to below 370 mAh g^{-1} after 100 cycles, while the S1005 showed superior capacity retention even after 300 cycles at the same current value, as shown in Fig. 6b. In addition, S1005 showed a high columbic efficiency of 99% that was maintained for up to 300 cycles at same current value, demonstrating that the evenly-distributed Fe_3O_4 nanoparticles surrounding carbon matrix had a high charge/discharge reversibility. The Fe_3O_4 nanoparticles in the carbon matrix may have been evenly distributed in poly(AN-co-TMSPM) matrix during polymerization because of the attractive interaction of the hydrogen atoms of citric acid on the surface of Fe_3O_4 nanoparticles with the electronegative atoms of TMSPM in medium. Thin carbon layers could be interspersed between all of the Fe_3O_4 nanoparticles, which can accommodate variation in volume of Fe_3O_4 nanoparticles; this protects against the aggregation of Fe_3O_4 nanoparticles during long cycling, and cycling performances and rate capability are consequently enhanced, as shown in Fig. 6a and b. In contrast, since S1010 had a porous structure, it could not prevent variation in the volume and aggregation of Fe_3O_4 nanoparticles in the composite microspheres during the lithium insertion and extraction process; consequently, rapid capacity fading was observed on cycling. These results indicate that the structural and morphological characteristics of Fe_3O_4/C composite microspheres affect electrochemical performances.

4. Conclusions

Fe_3O_4/C composite microspheres were synthesized by O/W suspension polymerization and heat treatment. It was confirmed that the morphology of the microspheres varied with the weight ratio of Fe_3O_4 nanoparticles to poly(AN-co-TMSPM) matrix. When used as anodes for LIBs, Fe_3O_4/C composite microspheres containing 72 wt.% Fe_3O_4 showed capacity retention of 91% after 300 cycles with columbic efficiency of 99% over all cycles due to high structural stability. On the other hand, Fe_3O_4/C composite microspheres containing 98 wt.% Fe_3O_4 nanoparticles showed severe capacity

fading with a poor rate capability due to their very small amount of carbon and its low electrical conductivity, porous structure. The electrochemical performance of the Fe_3O_4/C composite microspheres depends on the weight ratio of Fe_3O_4 nanoparticles to carbon matrix and their particle structure. It also demonstrates that Fe_3O_4/C composite microspheres that have high structural stability prevent agglomeration of Fe_3O_4 nanoparticles and the resulting capacity fading upon cycling.

Acknowledgments

This work was supported by the National Research Foundation of Korea (NRF) grant funded by the Korea government (MEST) (No. 2012-0002074).

Appendix A. Supplementary data

Supplementary data related to this article can be found at http://dx.doi.org/10.1016/j.jpowsour.2013.02.035.

References

[1] J.M. Tarascon, M. Armand, Nature 414 (2001) 359–367.
[2] P. Poizot, S. Laruelle, S. Grugeon, L. Dupont, J.M. Tarascon, Nature 407 (2000) 496–499.
[3] H. Zhou, S. Zhu, M. Hibino, I. Honma, M. Ichihara, Adv. Mater. 15 (2003) 2107–2111.
[4] P.L. Taberna, S. Mitra, P. Poizot, P. Simon, J.M. Tarascon, Nat. Mater. 5 (2006) 567–573.
[5] G. Derrien, J. Hassoun, S. Panero, B. Scrosati, Adv. Mater. 19 (2007) 2336–2340.
[6] Y. Yu, C.H. Chen, Y. Shi, Adv. Mater. 19 (2007) 993–997.
[7] W.M. Zhang, X.L. Wu, J.S. Hu, Y.G. Guo, L.J. Wan, Adv. Funct. Mater. 18 (2008) 3941–3946.
[8] T. Yoon, C. Chae, Y.K. Sun, X. Zhao, H.H. Kung, J.K. Lee, J. Mater. Chem. 21 (2011) 17325–17330.
[9] J.S. Chen, Y. Zhang, X.W. (David) Lou, ACS Appl. Mater. Interfaces 3 (2011) 3276–3279.
[10] P. Lianm, X. Zhu, H. Xiang, Z. Li, W. Yang, H. Wang, Electrochim. Acta 56 (2010) 834–840.
[11] Q. Hao, D. Lei, X. Yin, M. Zhang, S. Liu, Qiuhong Li, L. Chen, T. Wang, J. Solid State Electrochem. 15 (2010) 2563–2569.
[12] S. Wang, J. Zhang, C. Chen, J. Power Sources 195 (2010) 5379–5381.
[13] J.Z. Wang, C. Zhong, D. Wexler, N.H. Idris, Z.X. Wang, L.Q. Chen, H.K. Liu, Chem. Eur. J. 17 (2011) 661–667.
[14] S. Ni, D. He, X. Yang, T. Li, J. Alloys Compd. 509 (2011) L305–L307.
[15] J. Jamnik, J. Maier, Phys. Chem. Chem. Phys. 5 (2003) 5215–5220.
[16] Y. He, L. Huang, J.S. Cai, X.M. Zheng, S.G. Sun, Electrochim. Acta 55 (2010) 1140–1144.
[17] Y. Huang, Z. Dong, D. Jia, Z. Guo, W.II. Cho, Electrochim. Acta 56 (2011) 9233–9239.
[18] Y. Sahoo, A. Goodarzi, M.T. Swihart, T.Y. Ohulchanskyy, N. Kaur, E.P. Furlani, P.N. Prasad, J. Phys. Chem. B. 109 (2005) 3879–3885.
[19] M. Racuciu, D.E. Creanga, A. Airinei, Eur. Phys. J. E 21 (2006) 117–121.
[20] Y.Y. Yu, W.C. Chen, Mater. Chem. Phys. 82 (2003) 388–395.